RMetS
Royal Meteorological Society

Structure and dynamics of the convective boundary layer on Mars as inferred from large-eddy simulations and remote-sensing measurements

A. Spiga,[a,b]*F. Forget,[a] S. R. Lewis[b] and D. P. Hinson[c]

[a]*Laboratoire de Météorologie Dynamique, Institut Pierre-Simon Laplace, Université Pierre et Marie Curie, Paris, France*
[b]*Department of Physics and Astronomy, The Open University, Milton Keynes, UK*
[c]*Carl Sagan Center, SETI Institute, Mountain View, California, USA*
*Correspondence to: A. Spiga, Faculty of Science, Department of Physics and Astronomy, The Open University, Walton Hall, Milton Keynes MK7 6AA, UK. E-mail: a.spiga@open.ac.uk; spiga@lmd.jussieu.fr

The structure of the Martian convective boundary layer (BL) is decribed by means of a novel approach involving both modelling and data analysis. Mars Express radio-occultation (RO) temperature profiles are compared to large-eddy simulations (LESs) performed with the Martian mesoscale model. The model combines the Martian radiative transfer, soil and surface layer schemes designed at Laboratoire de Météorologie Dynamique (LMD) with the most recent version of the Weather Research and Forecast (WRF) fully compressible non-hydrostatic dynamical core. The key roles of the vertical resolution and, to lesser extent, of the domain horizontal extent have been investigated to ensure the robustness of the LES results. The dramatic regional variations of the BL depth are quantitatively reproduced by the Martian LES. Intense BL dynamics are found to underlie the measured depths (up to 9 km): vertical speed up to 20 m s^{-1}, heat flux up to 2.7 K m s^{-1} and turbulent kinetic energy up to 26 m^2 s^{-2}. Under specific conditions, both the model and the measurements show a distinctive positive correlation between surface topography and BL depth. Our interpretation is that, in the tenuous CO_2 Martian near-surface environment, the daytime BL is to first order controlled by the infrared radiative heating, fairly independent of elevation, which implies a simple correlation between the BL potential temperature and the inverse pressure ('pressure effect'). No prominent 'pressure effect' is in action on Earth where sensible heat flux dominates the BL energy budget. Both RO observations and numerical simulations confirm the terrain-following behaviour of near-surface temperature on Mars induced by the dominant radiative influence. The contribution of the Martian sensible heat flux is not negligible and results in a given isotherm in the BL being comparatively closer to the ground at higher surface elevation. The strong radiative control of the Martian convective BL implies a generalised formulation for the BL dimensionless quantities. Based on this formulation and the variety of simulated BL depths by the LES, new similarity relationships for the Martian convective BL in quasi-steady midday conditions are derived. Rigorous comparisons between the Martian and terrestrial BL and fast computations of the mean Martian BL turbulent statistics are now made possible by such similarity laws. Copyright © 2010 Royal Meteorological Society

Key Words: boundary layer; convection; Mars; large-eddy simulations; radio occultations; similarity laws

Received 6 August 2009; Revised 13 November 2009; Accepted 22 November 2009; Published online in Wiley InterScience 16 February 2010

Citation: Spiga A, Forget F, Lewis SR, Hinson D. 2010. Structure and dynamics of the convective boundary layer on Mars as inferred from large-eddy simulations and remote-sensing measurements. *Q. J. R. Meteorol. Soc.* **136**: 414–428. DOI:10.1002/qj.563

1. Introduction

The Martian boundary layer (BL) has received attention from scientists since space exploration began. Pioneering work in the 1960s and 1970s emphasised the crucial role of large diurnal variations of the ground temperature and low atmospheric thermal inertia and radiative time-scale (Goody and Belton, 1967). Such characteristics of the Martian environment are conducive to an ultra-stable shear-driven night-time BL and a deep convective daytime BL (Gierasch and Goody, 1968) with mixing heights exceeding the terrestrial values (Blumsack *et al.*, 1973; Pollack *et al.*, 1976).

In the late 1970s, an important milestone in Martian BL studies was reached with the *in situ* temperature and wind measurements made by the Viking landers. Martian near-surface diurnal temperature variations were found to be three times larger than those on Earth (Hess *et al.*, 1977) and the turbulent heat flux three times higher, despite a ratio between sensible flux and incoming solar flux an order of magnitude lower (Sutton *et al.*, 1978). Unprecedented observations of BL phenomena, such as cloud streets and dust devils, were carried out by the Viking Orbiter (Briggs *et al.*, 1977; Thomas and Gierasch, 1985).

The Viking BL measurements were refined in the late 1990s, when Pathfinder touched down on the Martian surface. Three temperature sensors on the Pathfinder mast yielded the first quantitative estimates of daytime super-adiabatic near-surface gradients (5–10 $\mathrm{K\,m^{-1}}$). Retrieval of the power spectrum of the Martian BL turbulence was made possible by the high-frequency acquisition time (Schofield *et al.*, 1997).

The 10-year-long Mars Global Surveyor (MGS) mission launched in 1996 provided a wealth of data but it was difficult to resolve the BL in many of the remotely sounded observations. The numerous Thermal Emission Spectrometer (TES) temperature vertical profiles were of insufficient vertical resolution in the BL (Smith *et al.*, 2001). Radio-occultation (RO) profiles with less than 1 km vertical resolution in the lower atmosphere were available (Hinson *et al.*, 1999), but the latitude and time coverage were not suitable for BL convection studies. The TES instrument, however, enabled high-resolution retrievals of soil thermal properties (albedo, thermal inertia). In addition, the Mars Orbiter Camera (MOC) on board MGS offered high-resolution images of convective clouds and dust devils (Malin and Edgett, 2001).

In parallel with new missions, modellers started to adapt to Mars some of the existing three-dimensional non-hydrostatic mesoscale models (Rafkin *et al.*, 2001). Of particular interest in BL studies is the use of such models for so-called large-eddy simulations (LESs): the grid spacing is lowered to a few tens of metres so as to resolve the larger turbulent eddies, responsible for most of the energy transport within the BL (Lilly, 1962). Just as the parametrised single-column models clarified the role of radiation in the Martian BL energy budget (Haberle *et al.*, 1993; Savijärvi, 1999), the first Martian LES induced a leap forward in understanding the BL dynamics on Mars.

Through LES, Michaels and Rafkin (2004) analysed the fine-scale structure of the Martian daytime BL, dominated by convective processes (the 'convective' BL): mixed-layer growth, polygonal cells, thermal updraughts and convective vortices. The last phenomenon was the focus of the Toigo *et al.* (2003) LES study which showed similarities between the modelled vortices and the observed Martian dust devils. These preliminary results were recently confirmed by other studies (Richardson *et al.*, 2007; Sorbjan, 2007; Spiga and Forget, 2009). LESs were also used to investigate atmospheric hazards during the entry, descent and landing (EDL) of the Mars Exploration Rovers (MER) (Rafkin and Michaels, 2003; Toigo and Richardson, 2003) and the Phoenix lander (Michaels and Rafkin, 2008; Tyler *et al.*, 2008).

To date, LES studies have mostly centred on idealised numerical experiments, which have produced plausible results with respect to the limited observations available. For instance, Michaels and Rafkin (2004) found that the horizontal structures of updraughts simulated in LES and convective clouds observed by MOC were similar. Spiga and Forget (2009) noticed encouraging agreement between LES results in Gusev Crater and MER miniTES temperature profiles up to 2 km above the surface (Smith *et al.*, 2006).

The quantitative validation of LES diagnostics against existing data remains to be done. One of the main limiting factors is the paucity of data covering the entire vertical extent of the Martian BL. This limitation was recently addressed with the Mars Express (MEx) RO profiles, obtained by Hinson *et al.* (2008, designated H08 below). The experiments conducted with MEx have provided good coverage at latitudes and local times (LTs) where BL convection is occurring. Properties such as the potential temperature down to 1 km above the surface, as well as the BL depth, can be determined accurately by the RO limb sounder. The vertical resolution is < 1 km (much smaller than typical BL depths on Mars) whereas the horizontal resolution is much larger. Such measurements enabled the authors of H08 to identify striking variations of the depth of the convective BL in the low-latitude Martian regions.

The purpose of the present study is to compare the H08 RO retrievals with LESs in order to propose an original description of the Martian convective BL. The data are employed to validate the model, which in turn helps to interpret the signatures identified in the data. To the extent of our knowledge, this is the first Martian BL study to propose a quantitative comparison between LES predictions and actual measurements.

2. Martian large-eddy simulations

LESs presented in this study are performed with the Martian Mesoscale/Microscale Model of Spiga and Forget (2009, designated SF09 below) developed in Laboratoire de Météorologie Dynamique (LMD). The model combines the Advanced Research Weather Research and Forecasting (ARW-WRF) fully compressible non-hydrostatic dynamical core (Skamarock and Klemp, 2008) with the comprehensive set of physical parametrisations for Martian dust, CO2, water and photochemistry cycles in the LMD Global Climate Model (GCM) (Forget *et al.*, 1999).

Martian planetary constants are used, notably acceleration due to gravity $g = 3.72\,\mathrm{m\,s^{-2}}$, specific heat capacity $c_p = 844\,\mathrm{J\,K^{-1}kg^{-1}}$ and gas constant $R = 192\,\mathrm{m^2\,s^{-2}K^{-1}}$. Potential temperature θ is defined with respect to the reference pressure value $p_0 = 610$ Pa in the Exner function $\Pi = (p/p_0)^{R/c_p} = T/\theta$ where T is absolute temperature (K) and p atmospheric pressure (Pa). Π is also named 'dimensionless pressure'.

Further details on the model can be found in SF09, as well as typical simulations (section 3.4: LES analyses in the Gusev Crater environment). For the present LES studies, several improvements were made to the Martian Mesoscale/Microscale Model described in SF09.

2.1. Dynamical core

Version 2.2.1 of the WRF dynamical core used in SF09 is replaced by version 3 released in April 2008. The new version of the dynamical core offers better handling of parallel computations with periodic boundary conditions (used in LESs to simulate the situation of an infinite flat plain), enhanced numerical stability, dedicated 'high-resolution' LES mode with simplified initialisation and a positive definite built-in advection scheme.

In the new LMD Martian LES model, subgrid-scale (SGS) turbulent mixing is not computed by the SF09 Mellor–Yamada 2.5-order (MY2.5) scheme; instead, strategy adopted by Moeng *et al.* (2007) for terrestrial LES with WRF is chosen. Firstly, mixing terms are evaluated in physical space (x,y,z) rather than along coordinate surfaces. Secondly, the three-dimensional SGS turbulent kinetic energy e (prognostic) is advected by the resolved motions in the LES and used to compute the horizontal and vertical mixing coefficients through a 1.5-order closure (Deardorff, 1980; Skamarock and Klemp, 2008). This SGS scheme is thought to yield better performance in describing afternoon mixed layers than the SF09 MY2.5 scheme (Stull, 1988).

2.2. Physical parametrisations

Physical parametrisations used for LESs in the present study are similar to those described in SF09 and references therein. Any SGS physical parametrisation specific to large-scale or mesoscale studies (convective adjustment, gravity wave drag) is turned off. Computations of radiative transfer by atmospheric CO_2 and dust are included, as well as predictions of surface temperature by a 10-layer soil model. Thus surface and radiative forcings are computed in the model at each physical timestep (30 s in this study). Modelled vertical profiles of radiative heating rates are qualitatively similar to those published in the literature (e.g. Figure 3 in Savijärvi *et al.*, 2004) and omitted here for the sake of brevity.

Uniform topography, albedo, thermal inertia in the domain are set to values measured by MGS instruments (SF09 give further references). Constant and horizontally uniform dust loading is prescribed in the model, with vertical distribution described in Forget *et al.* (1999) and MGS-derived altitude of dust-layer top described in Montmessin *et al.* (2004).

Surface layer values for sensible heat flux H_s and friction velocity u_* are passed on to the turbulent diffusion scheme where they modify momentum and potential temperature at lowest grid levels (Moeng *et al.*, 2007). Sensible heat flux H_s is evaluated by the bulk aerodynamic formula

$$H_s = \rho\, c_p\, u_*\, T_*\,, \qquad (1)$$

where ρ is atmospheric density. At each grid point and timestep, T_* is the temperature difference between surface and first atmospheric layer (at altitude z_1 above ground) and friction velocity u_* is the product between wind velocity in the first layer (background wind plus resolved turbulent winds) and von Kármán drag coefficient $C_d = [0.4/\ln(z_1/z_0)]^2$ with surface roughness $z_0 = 1$ cm. Altitudes of lowermost model layers are set 2, 10, 29, 62 m above ground so as to ensure fine vertical resolution in the Martian shallow surface layer.

2.3. Post-processing

All the displayed quantities in this paper (temperature profiles, turbulence statistics profiles) are horizontally averaged over the whole LES domain. Sufficient LES grid points are defined so that time (typically 1 h) and spatial averaging yield similar results, according to the ergodic principle (Stull, 1988).

The mean component (e.g. of potential temperature θ) is denoted $\langle\theta\rangle$ and the turbulent component is $\theta' = \theta - \langle\theta\rangle$. In order to compute the vertical eddy heat flux $\langle w'\theta'\rangle$ at a given timestep at each altitude, the mean temperature vertical profile $\langle\theta\rangle$ is first computed so as to calculate θ'. The product $w'\theta'$ on each grid point is then horizontally averaged in the whole domain to yield $\langle w'\theta'\rangle$. The same methodology is employed for the turbulent kinetic energy (TKE) $0.5\,[\langle u'^2\rangle + \langle v'^2\rangle + \langle w'^2\rangle]$. Note that the quantity we call here TKE for sake of brevity is the 'resolved convection' TKE. The TKE computed by the SGS parametrisation is not included in the TKE discussed in the paper (values of the SGS TKE are below 10% of the resolved TKE).

The depth of the convective BL z_i can be estimated by various methods, e.g. by evaluating the altitude at which vertical eddy heat flux is minimum. For the sake of comparison, we chose instead the method described in H08, in which the BL top z_i is defined as the altitude z above the local surface where static stability $S(z) = \mathrm{d}T/\mathrm{d}z + g/c_p$ first equals $1.5\,\mathrm{K\,m^{-1}}$ (T is the mean LES atmospheric temperature in K). Figure 3 below shows this criterion yields reasonable estimates of mixed-layer depths and Figure 10 below shows heat flux is a minimum at $z/z_i = 1$, as is the case by definition with the 'heat flux' criterion.

2.4. Sensitivity study

The total extent and resolution of the LES grid in the horizontal and in the vertical are known to influence the LES predictions. We carry out the same simulation of deep BL convection (case *c*, described below) with the distinct settings shown in Table I. To first order, the BL depth by the end of the afternoon is consistently predicted to be 7.5–8 km. The results are insensitive to the horizontal resolution (100 m with $\mathrm{d}t = 1.5$ s or 50 m with $\mathrm{d}t = 0.75$ s) in agreement with the conclusions of Michaels and Rafkin (2004) and Toigo *et al.* (2003). A close analysis of Table I however shows that a few other numerical settings do influence the results.

Despite case 5 sharing similar vertical resolution and extent with cases 3 and 4, its BL depth is 250 m lower due to a smaller horizontal domain extent. The convective deepening of the daytime BL is indeed coupled with a widening of the associated horizontal polygonal convective cells, scaled with the BL depth. Should the domain width be too low, the BL growth in the LES may be restrained by artefacts arising from the periodic nature of the domain. We however emphasise that only small differences are seen between 101×101 (case 4) and 145×145 (case 3) 100 m

Table I. Sensitivity of the modelled Martian boundary-layer depth z_i (average value between 1700 and 1730 LT) to the LES horizontal/vertical resolution, domain size and model top.

	Grid $N_x \times N_y \times N_z$	dx (m)	Δx (km)	dz (m)	Δz (km)	z_i (km)
1	181 × 181 × 201	50	9.0	60	12	7.77
2	145 × 145 × 201	50	7.2	60	12	7.79
3	145 × 145 × 201	100	14.4	75	15	7.79
4	101 × 101 × 201	100	10.0	75	15	7.75
5	73 × 73 × 201	100	7.2	75	15	7.54
6	145 × 145 × 201	100	14.4	100	20	7.64
7	145 × 145 × 101	100	14.4	120	12	7.59
8	241 × 241 × 151	100	24.0	100	15	7.58
9	101 × 101 × 151	100	10.0	100	15	7.59
10	73 × 73 × 151	100	7.2	100	15	7.60
11	45 × 45 × 71	100	4.4	140	10	7.18

Table II. Five LES simulations carried out for the purpose of comparison with RO profiles. The test cases are designated as in Hinson *et al.* (2008).

	L_s (°)	φ (°N)	λ (°E)	$\mathcal{T}$ (tiu)	A	T_s (K)	h (km)	p_s (Pa)
a	47.1	21.8	205.0	55	0.27	284	−3.9	868
b	51.2	13.7	204.6	50	0.30	280	−3.6	855
c	52.1	12.3	237.2	60	0.30	279	+2.5	483
i	47.8	20.6	74.0	300	0.13	279	−0.5	630
z	67.0	−10.2	236.6	42	0.28	268	+8.4	266

L_s is the areocentric longitude, φ is the north latitude, λ is the east longitude, $\mathcal{T}$ is the thermal inertia (1 tiu= 1 J m^{-2} K^{-1} s$^{-1/2}$), A is the albedo, T_s is the simulated maximum surface temperature (occurring between 1200 and 1300 LT), h is the topography with respect to the MGS Mars Orbiter Laser Altimeter (MOLA) zero datum and p_s is the surface pressure.

simulations. This suggests that, as long as the horizontal extent of the domain is larger than the maximum BL depth, the BL growth is accurately modelled by the LES. Even domain widths slightly lower than the BL depth (case 5, 73 × 73) eventually yield reasonable results (3% error). The same conclusion stands for the 50 m resolution simulations, for the results with 7 km (case 2) and 9 km (case 1) domains are similar.

Sensitivity to domain width is only observed if the vertical resolution, which seems to be the dominant factor, is fine enough. As is shown by cases 8, 9 and 10, even a large domain extent of 24 km would result in up to 200 m lower BL depth if the vertical resolution is too coarse. Changing the position of the model top (cases 6 and 7) has a relatively weak effect. We shall note that still the BL depth differences resulting from coarser vertical resolution are low. The computationally faster 73 × 73 × 151 predictions are within a few % of the reference 145 × 145 × 201 LES results.

Case 11 is an obviously inaccurate LES with low domain width and coarse vertical resolution. These extreme settings yield however a BL depth only 8% lower than case 2 (for a 10 times faster simulation). Moreover, the BL regional variations (Figure 2 below) are correctly accounted for even with this poor configuration. If the BL depth is < 6 km, the prediction is actually better than 8%, for the vertical resolution is the only limiting factor.

Although not reported in the table for the sake of brevity, the vertical velocity perturbations, the predicted vertical eddy heat flux and the temperature of the mixed layer are similar in all simulations. In addition, simulations starting at 1000 LT show negligible differences with the baseline 0800 LT LES.

As a conclusion, given the outcome of the present sensitivity study and the necessary trade-off between accuracy and computational cost, we define case 2 (145 × 145 × 201, 50 m LES with 12 km model top) as the reference configuration for the analysis that follows. Alternatively, our tests show that the nearly four times 'cheaper' configuration 4 (101 × 101 × 201, 100 m LES with 15 km model top) yields similar results, which may be useful if there are numerous test cases to address.

3. Evolution of the convective boundary layer

3.1. *Description of the case-studies*

The main conclusion of the H08 paper is the identification of dramatic regional contrasts of the depth of the convective BL on Mars. Authors of this study suggest that topography plays a dominant role in such regional variations (their Figure 6), at least when considering locations at constant latitude and LT. In the present study, our aim is to test whether these findings are supported by our Martian LES model.

In the light of those conclusions, we chose for LES five combinations of location and L_s thought as typical of the whole H08 dataset. Characteristics of these five case-studies are summarised in Table II. Considered locations are Amazonis Planitia (cases *a* and *b*), Tharsis (cases *c* and *z*) and Nili Fossae (case *i*). The season is northern spring in each case. For further reference, Table II reports the various soil

properties (topography, thermal inertia, albedo) in the five case-studies and the maximum daytime surface temperature predicted by the LMD Mesoscale/Microscale Model.

Each run is initialised at 0800 LT with a large-scale temperature profile extracted from the Mars Climate Database (MCD) version 4.3 (Millour *et al.*, 2008) corresponding to geographical coordinates and L_s indicated in Table II. MCD climatologies are based on LMD–GCM simulations with similar Martian physical parametrisations as in the LES carried out in this study. The same initial temperature profile is prescribed at every grid point and random 0.1 K perturbations are added to the lowest levels to kick off convection. Surface pressure p_s, a key parameter in the present study, is also obtained from MCD through 'high-resolution' calculations described in Forget *et al.* (2007, section 4.2).

Atmospheric dust loading and large-scale/mesoscale 'background' wind are known to influence the growth of the mixed layer. Contrasts of dust opacity are however low in Martian northern spring in regions where H08 measurements were carried out. Moreover, preliminary tests (not shown) suggest that typical regional variations of background wind induce changes in BL depths unlikely to account for the large variability observed by H08. Thus, for the sake of conciseness and simplicity, the present paper is based on windless 'free convection' LES with dust opacity $\tau = 0.3$. Further exploration of the sensitivity of convective BL properties to dust opacity and background wind is ongoing work.

3.2. General LES predictions for Mars

LES results in Figure 1 summarise the main characteristics of the Martian convective boundary layer (Michaels and Rafkin, 2004; Sorbjan, 2007; Tyler *et al.*, 2008; Spiga and Forget, 2009). Daytime evolutions of mixed-layer potential temperature, vertical velocity, vertical eddy heat flux and turbulent kinetic energy are shown in the example of case *b*. Martian daytime BL turbulence is about one order of magnitude more vigorous than its terrestrial counterpart: maximum vertical eddy heat flux and TKE predicted by the LMD Martian LES are respectively $1.2\,\mathrm{K\,m\,s^{-1}}$ and $10\,\mathrm{m^2\,s^{-2}}$. Peak vertical velocities are $12\,\mathrm{m\,s^{-1}}$ (updraughts) and $8\,\mathrm{m\,s^{-1}}$ (downdraughts, not shown in Figure 1).

Modelled BL depths in the five case-studies are displayed in Figure 2. As emphasised in previous studies, the daytime convective BL is significantly deeper on Mars than it is on Earth: typical Martian BL depths exceed extreme terrestrial values over desert regions (5 km). Around 1100 LT, the growing Martian mixed-layer already extends higher than its fully developed terrestrial counterpart in the typical example of BL convection over land in midlatitudes (1 to 2 km).

General facts about the Martian BL daytime growth in windless conditions can be inferred from LES results in Figures 1 and 2. Before 1000 LT, the BL depth slowly increases as the last remains of the strong nocturnal stable layer are 'burnt off'. After 1000 LT, the convective BL rapidly rises to reach a roughly constant depth at 1530 LT, which persists until the end of the afternoon at 1800 LT. Quasi-stationary state is reached later on Mars than on Earth, where constant depth is attained between 1200 and 1300 LT (Wilde *et al.*, 1985). Interestingly, LESs suggest that the BL vertical extent is still close to its maximum when the RO measurements were done at 1700 LT, which is therefore an optimal LT for BL studies.

3.3. Modelled and observed BL depths

3.3.1. Qualitative behaviour: the 'pressure effect'

Figure 2 shows that dramatic regional variations of convective BL depth are predicted by the LMD Martian LES. Local topography strongly influences the daytime BL growth. Although cases *b* in low Amazonis plains and *c* in high Tharsis plateaux share similar surface temperatures (owing to similar insolation conditions and soil thermal properties), the latter exhibits BL depths 2.5 to 3 km higher than the former. Comparisons between cases *b* and *i* yield the same conclusion, as both surface temperatures are similar despite distinct insolation, albedo and thermal inertia (model predictions for surface temperature at 1400 LT are supported by TES data in Figure 8 of H08).

BL convection on Mars appears appreciably influenced by surface temperature only in cases where the topographical contrast is low. For instance, case *a* is about 200 m lower than case *b* but its convective BL is deeper owing to the higher surface temperature. Comparing case *z* to case *c* provides additional clues on how topography exerts a strong control on the BL depth and how surface temperature only acts as a second-order influence. Local surface in case *z* is 10 K colder and 6 km higher; the result of these two competing effects is a BL depth 1 km higher.

Thus, regional variability of BL depths modelled through LES is consistent with H08 diagnostics, showing a clear correlation with spatial variations in surface elevation and a weaker dependence on spatial variations in surface temperature. According to H08, such behaviour is related to *convection aris[ing] from solar heating of the ground, and the impact of this heat source on thermal structure [being] largest where the surface pressure [... is] smallest, at high surface elevations*.

Consider indeed a point at the bottom of the mixed layer or, equivalently, at the top of the surface layer (typically a few tens of metres above ground). Values of pressure p and potential temperature θ are close to values of surface pressure and mixed-layer potential temperature. We assume that regional variations of pressure p only arise from contrasts in elevation. Evolution of θ with time t is given by the second law of thermodynamics

$$c_p \frac{\mathrm{d}\theta}{\mathrm{d}t} = \Pi^{-1} \mathcal{J}, \tag{2}$$

where $\mathcal{J}$ is the total atmospheric heating rate in $\mathrm{K\ s^{-1}}$. Equation (2) states that regional variations in θ originate from regional variations in (i) total heating rate $\mathcal{J}$ and (ii) dimensionless pressure Π. We propose to refer to point (ii) as the 'pressure effect'.

If heating rates $\mathcal{J}$ are similar in two locations, the 'pressure effect' causes mixed-layer potential temperatures to be larger where pressure is lower, at higher elevations. Convective plumes then rise higher in the free atmosphere so as to find a layer of equal potential temperature where their buoyancies reach zero: in other words, convective available potential energy of BL convective plumes is larger. Thus, the 'pressure effect' is likely to account for deeper modelled and observed BL in Tharsis plateaux than in Amazonis plains. Reasons why Martian conditions are conducive to this effect being prominent are detailed in section 4.

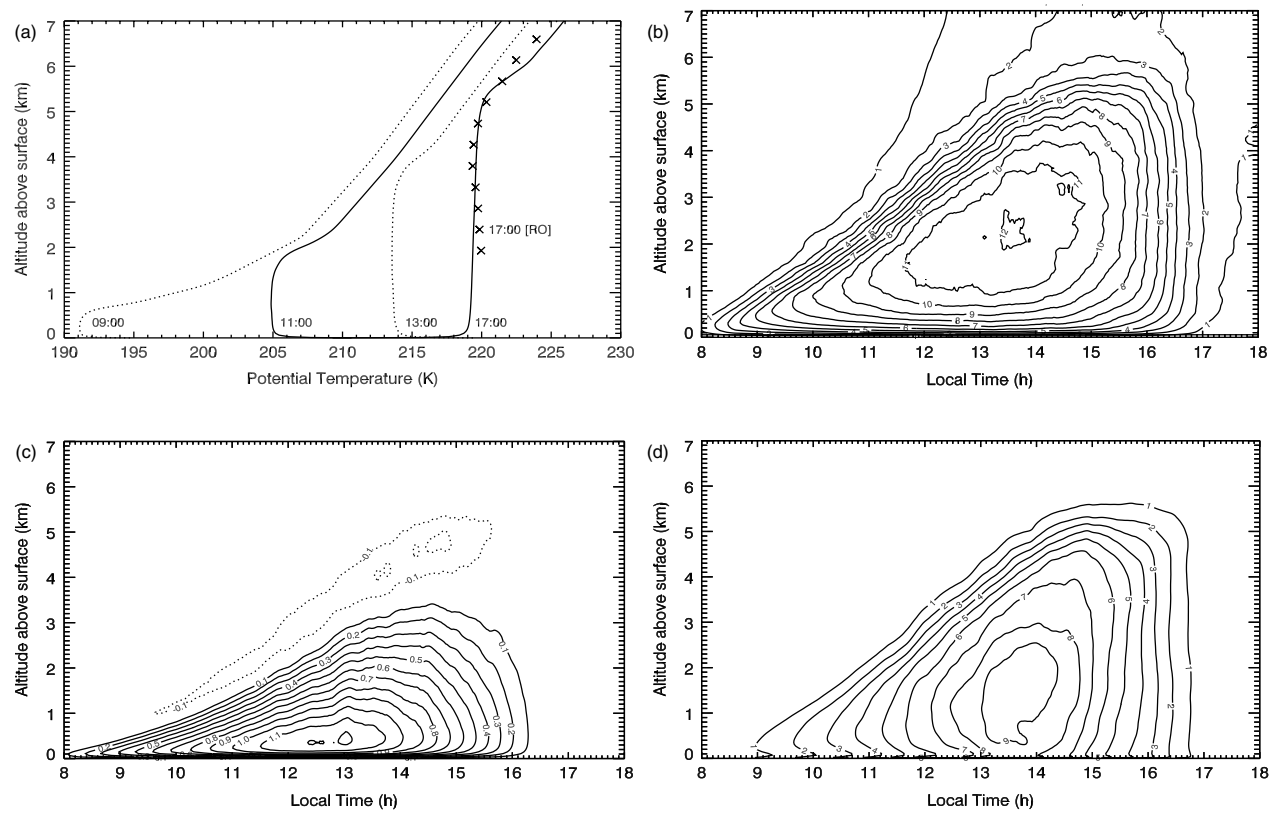

Figure 1. Variation of the LES statistics with time and height above ground in case-study *b* (Amazonis Planitia): (a) potential temperature (K) with superimposed radio-occultation profile at 1700 LT, (b) updraught maximum vertical velocity ($m\,s^{-1}$), (c) vertical eddy heat flux ($K\,m\,s^{-1}$), and (d) turbulent kinetic energy ($m^2 s^{-2}$). All displayed quantities in this article are averaged over the simulation domain.

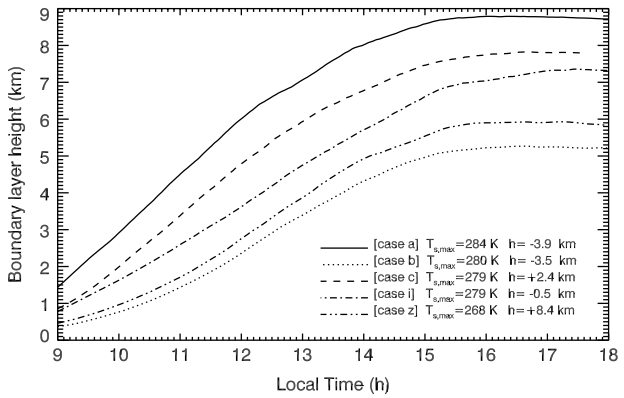

Figure 2. Variations of the boundary-layer depth above the local surface with time for the five LES case-studies. h and T_s are defined in Table II.

3.3.2. *Quantitative comparisons*

Regional variability of the BL identified in the RO data is also quantitatively confirmed by the complementary modelling approach. This is suggested for case *b* in Figure 1 where the H08 potential temperature profile at 1700 LT is superimposed on the LES predicted profile. Figure 3 shows that both potential temperature and depth of the mixed layer measured by H08 for cases *a*, *b*, *c* are accurately reproduced by the LMD Martian LES. Differences between BL depths in the LES and in the RO at 1700 LT are below 500 m. Predicted potential temperature of the mixed-layer is within 2 K of the H08 value.

As most of the BL turbulent transport is resolved explicitly by the LES and not parametrised, such results represent a validation of the LES dynamics and their coupling to the LMD Martian physics. The mixed-layer potential temperature and the BL depth at 1700 LT result from the LES step-by-step integration of the afternoon BL growth. We thus believe that the whole process of boundary-layer growth during the day, illustrated in Figure 2, is consistent with producing plausible BL potential temperatures and depths at the end of the afternoon.

This overall agreement should not conceal some interesting differences in the modelled and observed profiles. Notably, in Figure 3 the increase of static stability S at the top of the boundary layer is steeper in the model than in the data. This difference could be due to various factors. On the measurements side, the figure shows that the RO vertical resolution might not permit an accurate description of the steep transition at the top of the BL. In addition, the RO profiles have to be regarded as an average over a roughly 400 km wide horizontal area on the planet. On the modelling side, large-scale and mesoscale phenomena leading to static stability variations are not taken into account in the idealised LES.

The good agreement between LES and RO profiles identified in cases *a*, *b*, *c* is not found in cases *i* and *z* displayed in Figure 4. In addition to the aforementioned possible limitations, the *i* and *z* RO profiles were acquired in areas of steep topographical gradients. Thus the discrepancy between LES and RO is linked to the peculiarity of such cases and is not necessarily indicative of generic model or data retrieval flaws.

Case *i* is located in Nili Fossae in the vicinity of the sharp topographical transition to Isidis Planitia. It is thus difficult to evaluate the topographical reference in this case. The fact that the profile ends higher than the regular ~ 1 km above

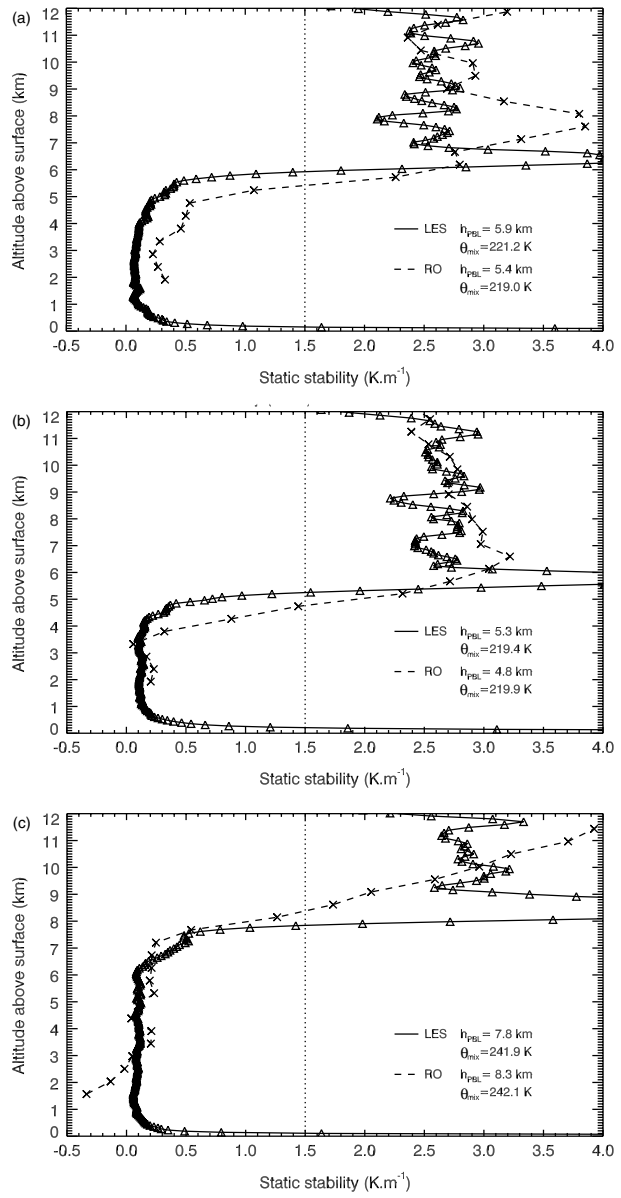

Figure 3. Vertical profiles of static stability at 1700 LT predicted by the LES (full lines and triangles) and the radio-occultation measurements (dashed lines and crosses) for cases *a*, *b* and *c*. The boundary-layer depths and the mixed-layer potential temperatures are shown. Note that, for the sake of consistency, height above the surface is obtained by upward integration of the hydrostatic equation, using the (simulated and measured) temperature and pressure profiles.

the ground is doubtful. Thus, the distinct BL depths in the LES and in the RO might result from a discrepancy in the altitude reference. This conclusion is further supported by similar mixed-layer potential temperatures in both cases. Large-scale and mesoscale circulations not resolved by the LES might however also play a role (section 4.3).

The case *z* is located on the rims of Arsia Mons. Difficulties described in the previous paragraph also apply, though the situation is even more complex. The presence of the mountain is usually associated with gravity waves which might induce mixed layers when undergoing breaking. The good agreement in BL depth between the LES and the RO is only apparent as the variations of RO static stability near the top of the convective BL top are ambiguous. This is confirmed by the lack of agreement between the modelled and the observed mixed-layer potential temperatures.

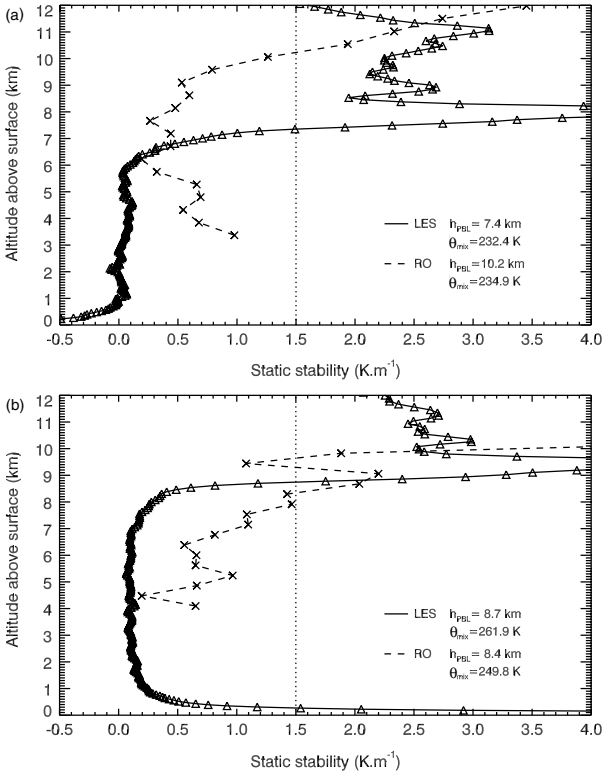

Figure 4. As Figure 3, but for cases (a) *i* and (b) *z*.

3.4. *Regional variability in BL dynamics*

Validation of LES BL depth predictions against RO measurements (at least in three cases) is a step toward a better understanding of the Martian convective BL. High-resolution numerical modelling complements the RO observations acquired on a considerably larger area than the width of typical convective cells. The model offers a wealth of diagnostics not available in the data (cf. Figure 1) which enables us to get insights into the BL dynamics associated with regional differences in BL depth. Daytime evolutions of mixed-layer potential temperature, vertical velocity extrema, maximum vertical eddy heat flux and turbulent kinetic energy are compared for the five case-studies in Figure 5.

Figure 3 indicates that both data and LES support the fact that the higher the potential temperature, the deeper the BL, in agreement with theoretical arguments developed in section 3.3.1. Figure 5 shows that the picture drawn by the BL statistics during the whole daytime development of the convective BL is similar. A warmer BL (in the sense of potential temperature) undergoes enhanced diabatic warming that results in more vigorous turbulent heat flux $\langle w'\theta'\rangle$. The buoyancy flux, $g\langle w'\theta'\rangle/\theta$, induces larger variations of TKE, according to the TKE equation, hence higher vertical entrainment velocity w_e and thus deeper BL. In addition, the temporal evolution $\dot{z}_i$ of the BL depth is to first order $\dot{z}_i \approx w_e$. This is consistent with the BL growing comparatively faster in case *c* than in case *b* (Figure 2).

Our LESs demonstrate the high variability of the Martian BL dynamics associated with the regional contrasts of BL depth. Compare case *b* with case *z*, where the BL is nearly 4 km deeper. In this extreme situation, BL temperature is 50 K warmer, heat flux is more than doubled, TKE is

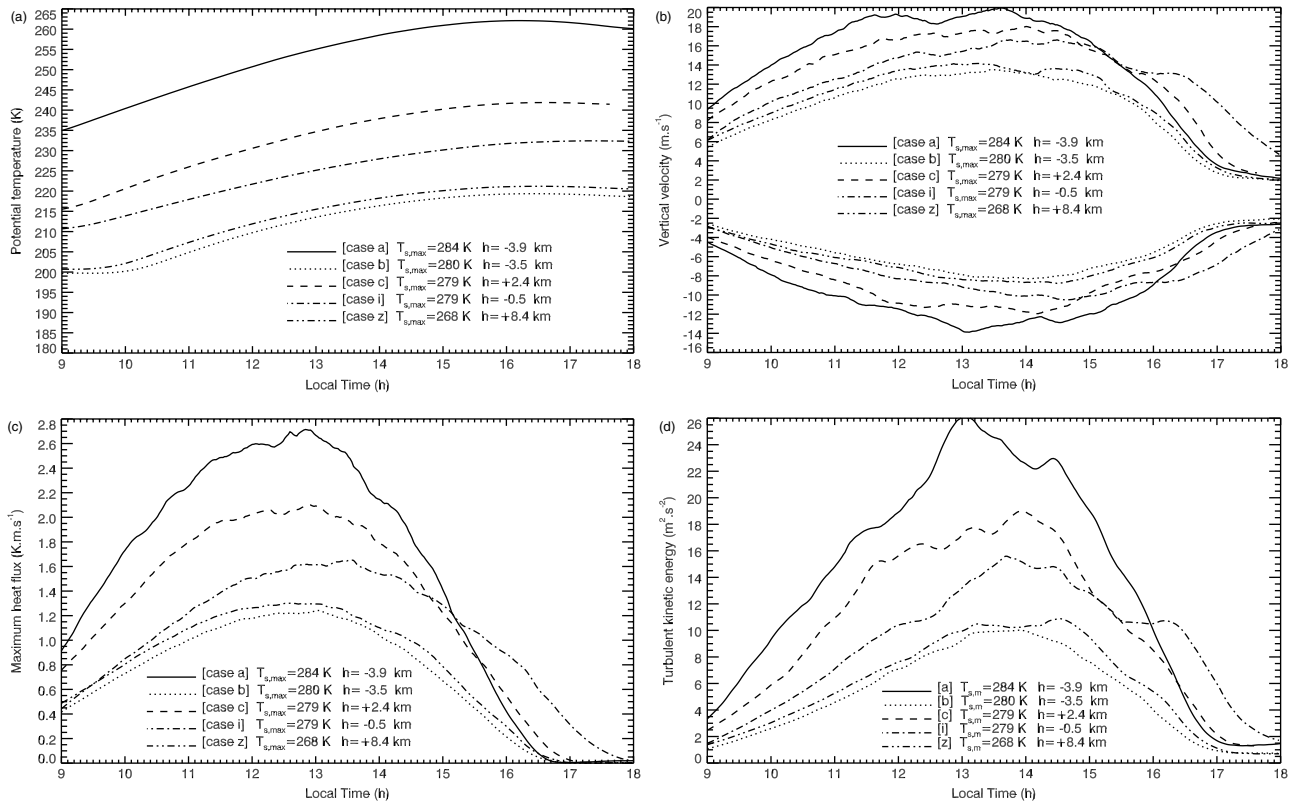

Figure 5. Variation of the LES statistics with time in the five case-studies defined in Table II. (a) Mixed-layer potential temperature (K), (b) updraught/downdraught maximum vertical velocity ($\mathrm{m\,s^{-1}}$), (c) maximum vertical eddy heat flux ($\mathrm{K\,m\,s^{-1}}$), and (d) maximum turbulent kinetic energy ($\mathrm{m^2 s^{-2}}$).

nearly tripled and updraughts reach $20\,\mathrm{m\,s^{-1}}$ between 1300 and 1400 LT. It is fortunate that, for other reasons than the BL turbulence concern, previous Martian spacecraft exclusively landed in low-altitude terrains! Vertical motions problematic for most EDL systems (over 7–8 $\mathrm{m\,s^{-1}}$) might actually be reached even in lower terrains (Tyler *et al.*, 2008).

As a final remark, we note in Figure 2 that the evolution of the BL depth maximum in case *i* is 'delayed' relative to the other cases. This phenomenon is actually easier to detect in the vertical eddy heat flux or in the vertical velocity extrema of Figure 3. It is consistent with higher thermal inertia of Nili Fossae terrains which causes the daily peak and drop of surface temperature to be shifted towards later LTs. Thus the maximum vertical velocity is still $\sim 8\,\mathrm{m\,s^{-1}}$ at 1700 LT in case *i*, whereas in the other cases it is below $3\,\mathrm{m\,s^{-1}}$. At the end of the afternoon, the most turbulent situation does not correspond to the deepest BL. The example of case *i* exemplifies that the role of the soil properties should not be forgotten although our findings, along with H08, suggest a significant topography control on the BL dynamics.

4. Energetics of the convective boundary layer

Section 3.3.1 gives the basic principles of the 'pressure effect'. In this section, we further describe the daytime BL energetics on Mars and on the Earth, the likelihood of 'pressure effect' on both planets, as well as causes and consequences of the BL being significantly warmer at higher altitudes on Mars both in RO and in LES.

4.1. *Energy budget on Mars and on the Earth*

The starting point is Eq. (2), written as in section 3.3.1 at constant altitude above the surface. In a given region, differences of elevation between two distinct points are identified through differences of dimensionless pressure Π. The bottom of the mixed layer (or equivalently the top of the surface layer) is considered, so that potential temperature θ is approximately equal to the mixed-layer value.

In daytime conditions, the atmospheric heating rate $\mathcal{J}$ in Eq. (2) comprises three terms: $\mathcal{J}_{\mathrm{LH}}$ the condensation/evaporation energy transfers, $\mathcal{J}_{\mathrm{LW}}$ the divergence of net infrared radiative flux and $\mathcal{J}_{\mathrm{SW}}$ the divergence of net short-wave radiative flux. In free convection conditions, to first order after Reynolds averaging (section 2.3), the advection term in the left-hand side reduces to vertical divergence of vertical eddy heat flux $\langle w'\theta'\rangle$ (e.g. Savijärvi, 1999). Hence the law of evolution of mixed-layer potential temperature θ:

$$c_p \frac{\partial \theta}{\partial t} = \Pi^{-1}\left(\mathcal{J}_{\mathrm{LH}} + \mathcal{J}_{\mathrm{LW}} + \mathcal{J}_{\mathrm{SW}}\right) - c_p \frac{\partial \langle w'\theta'\rangle}{\partial z}. \qquad (3)$$

Since considered points are located at a small distance dz above the surface-layer top, we have $\rho\, c_p\, \mathrm{d}\langle w'\theta'\rangle \approx \rho\, c_p\, \langle w'\theta'\rangle_z - H_{\mathrm{s}}$ where H_{s} is the effective sensible heat flux, i.e. the combination of molecular transfer from a heated surface in the microlayer and small-scale turbulent transport in the surface layer, of which Eq. (1) is one possible parametrisation.

4.1.1. *The terrestrial case*

On Earth, the sensible flux H_{s} is overwhelmingly dominant (e.g. 20% of the incoming solar flux in terrestrial deserts).

The latent component $\mathcal{J}_{\rm LH}$ can be of importance outside arid regions. In contrast to these two terms, the radiative contribution $\mathcal{J}_{\rm LW} + \mathcal{J}_{\rm SW}$ is negligible, except in rare cases (e.g. Tibetan Plateau; Smith and Shi, 1992). Thus, in terrestrial arid regions, atmospheric heating rate $\mathcal{J}$ is approximately zero. A notable consequence of Eq. (3) is that no 'pressure effect' is in action in such conditions. Mixed-layer potential temperature is given by

$$c_p \frac{\partial \theta}{\partial t} \approx -\frac{\partial \langle w'\theta' \rangle}{\partial z}. \quad (4)$$

Regional variations of daytime potential temperature on Earth are mostly caused by contrasts in sensible flux $H_{\rm s}$. The main variable accounting for those regional variations is the surface temperature $T_{\rm s}$ controlled by insolation, soil properties and elevation. Terrestrial conditions are not generally conducive to higher potential temperatures in the daytime BL at higher elevations. In daytime conditions on Earth, the sensible heat flux significantly contributes to the surface budget and easily exceeds 50% of the net radiation at the surface. Consequently, surface temperatures are lower on mountains than in lower plains, insolation and soil type being similar. Mixed-layer potential temperature follows the same trend as the sensible heat flux $H_{\rm s}$ according to Eq. (4), because divergence of turbulent heat flux is negative in the terrestrial mixed layer (section 5.2 and Figure 11 below); on Earth $\langle w'\theta' \rangle$ decreases with altitude above ground.

4.1.2. *The Martian case*

The energy budget at the base of the Martian BL is distinct from the terrestrial one. Firstly, owing to the low atmospheric density and thermal inertia, the sensible heat flux $H_{\rm s}$ is only 2% of the incoming solar flux (Sutton *et al.*, 1978). Secondly, low values of Martian specific humidity cause $\mathcal{J}_{\rm LH}^{\rm H_2O}$ to be negligible (Savijärvi, 1999) and low CO_2 condensation temperatures imply that $\mathcal{J}_{\rm LH}^{\rm CO_2}$ is negligible outside polar regions. Thirdly, predominance of CO_2 and dust in the thin Martian atmosphere results in significant radiative contributions $\mathcal{J}_{\rm LW}$ and $\mathcal{J}_{\rm SW}$.

Up to several 100s of metres above ground, $\mathcal{J}_{\rm LW}$ is the dominant heat source in the Martian BL between 0900 and 1600 LT (Haberle *et al.*, 1993). Indeed, upwelling thermal infrared radiation from the insolated soil is prone to strong net absorption by the colder atmospheric CO_2 and, to lesser extent, H_2O and dust (Savijärvi, 1999). The direct absorption of incoming solar radiation in the visible by the atmospheric dust represents the main contribution to $\mathcal{J}_{\rm SW}$. This yields a constant warming with altitude in the BL as the dust can broadly be considered as well-mixed in convective conditions (Figure 20 of Haberle *et al.*, 1993). Except in very dusty conditions, $\mathcal{J}_{\rm SW}$ is however less crucial than $\mathcal{J}_{\rm LW}$ in the convective BL energy budget.

Thus, to first order, $\mathcal{J} \sim \mathcal{J}_{\rm LW}$ in the Martian environment and mixed-layer potential temperature is given by

$$c_p \frac{\partial \theta}{\partial t} \approx \Pi^{-1} \mathcal{J}_{\rm LW}\,. \quad (5)$$

(As is detailed in section 4.2, neglecting the turbulent heat term is a severe approximation but does not change the conclusions in this section.) Surface temperature controls the daytime BL potential temperature on Mars, as is the case on Earth, but for distinct reasons. In great contrast to terrestrial conditions, the Martian BL is strongly influenced by radiation. As suggested by Eqs. (2) or (5), the 'pressure effect' merely controls BL potential temperature if the dominant contribution to $\mathcal{J}$ is independent of dimensionless pressure Π (i.e. elevation). This is exactly what occurs with the dominant infrared radiative heating $\mathcal{J}_{\rm LW}$ of the Martian BL.

Consider indeed two locations with distinct altitudes but similar soil properties and insolation conditions–e.g. case *b* in Amazonis and case *c* in Tharsis (section 3 and Figure 3). The Martian surface is close to radiative equilibrium, as the influence of sensible and latent heat fluxes is negligible in the soil energy budget. Hence, regardless of the difference in altitude, values of surface temperature $T_{\rm s}$ are similar in low plains (Amazonis) and in high plateaux (Tharsis). Moreover, in the thin Martian near-surface CO_2 atmosphere, variations of the absorbed radiative energy in the infrared with pressure are negligible (e.g. Goody and Belton, 1967). As a consequence, infrared heating rate $\mathcal{J}_{\rm LW}$, and to first-order atmospheric BL heating rate $\mathcal{J}$, are similar in the two locations.

In contrast to the Earth, owing to the strong radiative control of the Martian BL, correlation between BL potential temperature and elevation is likely to originate on Mars from the 'pressure effect'. Both H08 data and LES results indicate that the daytime BL potential temperature is larger in the Tharsis case *c* than in the Amazonis case *b* (Figure 3). Figure 6 complements these diagnostics by showing the higher derivatives $\partial\theta/\partial t$ for case *c* where the pressure is lower. The quantity $c_p\,\Pi\,\partial\theta/\partial t$ is similar in cases *b* and *c* between 1200 and 1500 LT, which is expected from Eq. (5) and $\mathcal{J}_b \sim \mathcal{J}_c$.

Figure 6 also shows that the highest $\partial\theta/\partial t$ is obtained in case *z* over the coldest surface of the five cases. Owing to the high elevation of *z*, the 'pressure effect' overcomes here the influence of the difference in T_s resulting from albedo, thermal inertia or insolation variations. That is not always the case. Consider cases *i* and *b*. Lower $\partial\theta/\partial t$ in case *i* before 1400 LT results from larger thermal inertia ($\mathcal{J}_i < \mathcal{J}_b$ in Eq. (5)) rather than higher elevation (${\Pi_i}^{-1} > {\Pi_b}^{-1}$). This case confirms (1) the need for Martian LES with complete radiative transfer and soil model (section 2.2) and (2) the probably difficult identification of the correlation between BL depth and topography in the RO out of the spring

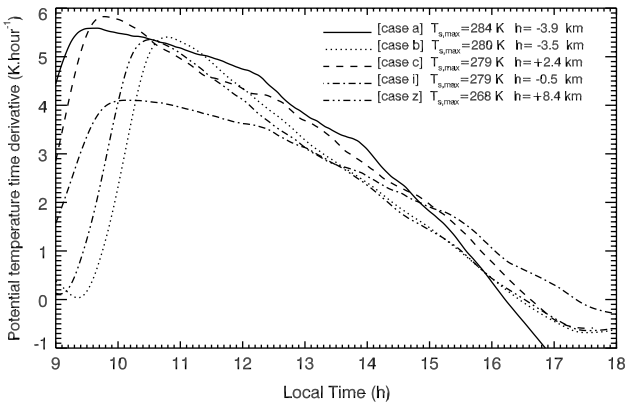

Figure 6. Variation of the time derivative of the mixed-layer potential temperature ($\mathrm{K\,h^{-1}}$) with time for the five LES case-studies. Note that before 1000 LT the behaviour is still influenced by the 'burning-off' of the remains of the night-time inversion.

hemisphere where T_s varies within a small range (Figure 8 in H08).

4.2. *Thermal structure of the Martian lower troposphere*

RO data cannot enable us to calculate $\theta(t)$ or $\partial\theta/\partial t$ so as to offer a 'ground-truth' confirmation of the preceding scenario. We relied instead, given the correct reproduction of the BL depth against the H08 data, on the modelled growth of daytime BL through LES.

Notwithstanding, assuming negligible meteorological variation of Π between t_1 and t_2, integration of Eq. (5) between sunrise (t_1) and sunset (t_2) yields

$$\theta_2 = \mathcal{A}\,\Pi^{-1}, \quad \text{with} \quad \mathcal{A} = T_1 + \int_{t_1}^{t_2} \frac{\mathcal{J}_{\mathrm{LW}}}{c_p}\,\mathrm{d}t\,, \qquad (6)$$

where θ_i and $T_i = \Pi\,\theta_i$ denotes potential and absolute temperature at time t_i at constant height above ground. Equation (6) is useful because mixed-layer potential temperature θ_2 at $t_2 \sim 1700$ LT is both measured by the H08 RO and predicted by the LES resolved convection. Sunrise is chosen for integration boundary t_1 because regional variability of absolute temperature T_1 at the bottom of the mixed layer at this time of day is often low. MCD climatologies derived from LMD–GCM predictions show that T_1 is approximately constant in regions (subtropics) and dates (northern spring) spanned by RO measurements.

In section 4.1, we describe how the Martian BL is controlled by radiation, which causes both surface temperature and atmospheric heating rate $\mathcal{J}$ to be independent of elevation, or equivalently dimensionless pressure Π. According to Eq. (6), potential temperature θ_2 is then approximately proportional to Π^{-1} on Mars, which is another expression of the 'pressure effect'.

LES results in Figure 7(a) show indeed that θ_2 follows a fairly robust linear trend with Π^{-1}:

$$\theta_2 = \alpha\,\Pi^{-1} + \beta\,. \qquad (7)$$

Interestingly, the LES linear trend is further evidenced by the H08 measurements with consistent α and β coefficients. This can be seen in Figure 7(b) showing the data in the $[\theta_2, \Pi^{-1}]$ frame for a large variety of soil properties, insolation and topography. (Note that the considered altitude above local surface is ~ 1 km instead of the bottom of the mixed layer which is not reached by the measurements.) The approximate linear behaviour of θ_2 with Π^{-1} in RO measurements and LES results tends to confirm that the 'pressure effect' is a dominant control of the BL daytime potential temperature in regions where H08 remote-sensing data were acquired.

Both measurements and simulations indicate that θ_2 is not proportional to the inverse dimensionless pressure Π^{-1}. Our interpretation of $\beta \neq 0$ in Eq. (7) is that the contribution of the divergence of the turbulent heat flux is not as prominent on Mars as it is on Earth, but still influences the BL energy budget (without being affected by the 'pressure effect'). Equation (5) should be replaced by

$$c_p\,\frac{\partial\theta}{\partial t} \approx \Pi^{-1}\mathcal{J}_{\mathrm{LW}} - c_p\,\frac{\partial\langle w'\theta'\rangle}{\partial z}. \qquad (8)$$

The modified version of Eq. (6) is

$$\theta_2 = \mathcal{A}\,\Pi^{-1} + \mathcal{B}, \quad \text{with} \quad \mathcal{B} = -\int_{t_1}^{t_2} \frac{\partial\langle w'\theta'\rangle}{\partial z}\,\mathrm{d}t\,. \qquad (9)$$

Equation (7) supported by LES predictions and RO measurements indicates that, to first order, both $\mathcal{A}$ and $\mathcal{B}$ are constants in Eq. (9). Slope α can be associated with radiative forcing $\mathcal{A}$ and y-intercept β to turbulent mixing $\mathcal{B}$ in the Martian BL. Figure 7 suggests that relative contributions to the potential temperature $\sim$ 1 km above the surface are 2/3 for radiation and 1/3 for mixing.

The sign of $\mathcal{B}$ deserves comment, because the Martian situation described by Eq. (8) is more complex than the terrestrial situation described by Eq. (4) (section 5.2 and Figure 11 below provide dimensionless analysis). Martian turbulent motions mix heat in the BL to counteract the strong radiative forcing. As shown in Figure 1, up to a few hundreds of metres above the ground, vertical divergence of vertical eddy heat flux $\partial\langle w'\theta'\rangle/\partial z$ is positive: radiative heat is removed from the lowermost levels of the BL and transported upward. The equivalent of Figure 7(a) near the surface indicates a negative value for $\mathcal{B}$. Higher up in the Martian BL, vertical eddy heat flux $\langle w'\theta'\rangle$ decreases with height, as is the case on Earth, which explains the positive value for $\mathcal{B} > 0$ in Figure 7.

Equations (7) and (9) can be written for absolute temperature

$$T_2 = \mathcal{A} + \mathcal{B}\,\Pi \qquad (10)$$

in order to better describe how LES and RO results give insights into the thermal structure of the Martian lower troposphere. Consider a constant level above the surface in the mixed layer, not too close to the surface so that $\mathcal{B} > 0$. Under the influence of radiation alone ($\mathcal{A}$ term in Eq. (10)), no regional variations of absolute temperature T_2 are expected if soil thermal properties do not vary too much. Additional influence of turbulent heat transfers ($\mathcal{B}$ term in Eq. (10)) imply higher temperatures than expected through the 'purely radiative' calculations. This influence is less pronounced over mountains where Π is lower. In other words, a given isotherm in the BL adopts mostly a terrain-following behaviour, but is closer to the ground over mountains.

Thermal structure obtained through high-resolution GCM simulations (Figure 8) with parametrised BL processes is consistent with diagnostics from H08 measurements and LES results. (Note that complete validation of GCM predictions remains out of the scope of the present paper.) Consider for instance the 205 K isotherm. GCM predicts that surface temperature differences are very low in the region, in accordance with section 4.1.2. Should radiative control be overwhelmingly dominant (Eq. (6)), the 205 K isotherm would be at constant height above ground in Figure 8. Instead, owing to the influence of turbulent mixing (Eq. (9)), it is closer to the surface over the mountain than it is over lower plains.

4.3. *Discussion*

Unsurprisingly, although the agreement between the (idealised) LES and data slopes is reasonable, the dispersion of the data in Figure 7 is significant. This dispersion might arise from observational artefacts or phenomena not accounted for in our preceding scenario.

Firstly, for locations at similar topography (thus similar p), distinct soil properties and insolation conditions yield different infrared and sensible contributions. In other words,

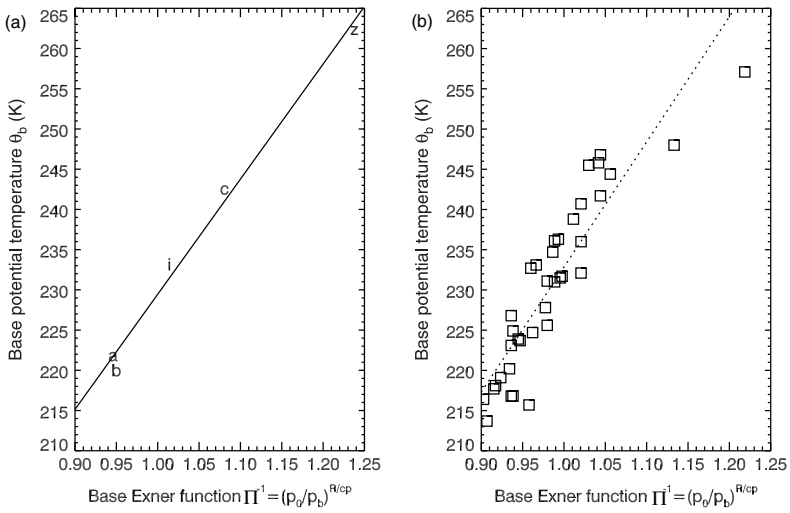

Figure 7. Mixed-layer potential temperature 1 km above the surface at 1700 LT as a function of the inverse dimensionless pressure Π^{-1} at the same time and height: (a) the five LES case-studies with $\theta = 143\ \Pi^{-1} + 86$ linear fit and (b) all the RO measurements carried out in *Hinson et al.* (2008) with $\theta = 156\ \Pi^{-1} + 77$ linear fit.

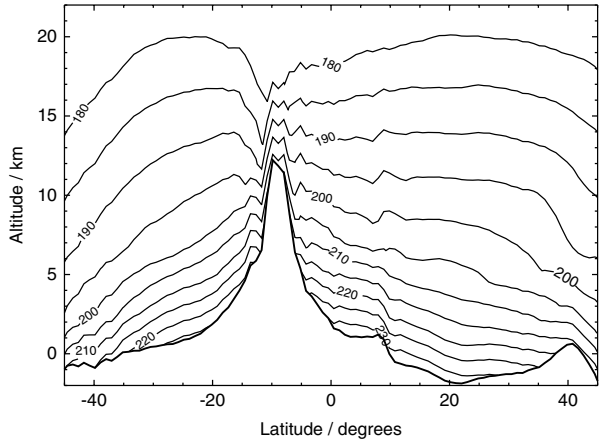

Figure 8. Latitude–altitude cross-section of absolute temperature at longitude 240°E. Predictions by the UK spectral version of the European Mars GCM (Forget *et al.*, 1999; Lewis and Read, 2003) run at very high resolution (T170, i.e. grid spacing below 1° latitude and longitude). Altitude is expressed above the MOLA zero-datum reference. The LT is 1600. The displayed field is an average over 10 Martian days at $L_s = 0°$ (northern spring equinox).

regional variations of $\mathcal{J}$ in Eq. (6) cannot be totally neglected. Secondly, large-scale and mesoscale winds (not taken into account in the LES) might enhance the influence of the sensible heat flux H_s (Ye *et al.*, 1990). Thirdly, regional and seasonal contrasts in dust opacity, as well as departures from the well-mixed assumption, result in a distinct shortwave term $\mathcal{J}_{SW}$. Fourthly, the meteorological variations of p during the afternoon cannot be neglected compared to the topography-induced variations, contrary to what is assumed in this paper. On Mars, thermal tides induce p perturbations up to 35 Pa and baroclinic waves up to 60 Pa.

Lastly, it is worth emphasising the focus of this section 4 on the BL potential temperature θ rather than the BL depth z_i. As is discussed in sections 3.3.1 and 3.4, higher θ usually means higher z_i. Large-scale and mesoscale variations of atmospheric stratification ('background' θ field) might however alter this simplified statement. Equivalently, the BL depth evolution given in section 3.4 is in fact $\dot{z}_i = w_e + w_b$, where w_b is the synoptic and mesoscale vertical velocity. Despite this meteorological control at larger scales than the BL convection, positive correlations for $z_i = f(\theta_2)$ and $z_i = f(\Pi^{-1})$ are observed in the H08 RO (albeit with large dispersion; figures not shown for sake of brevity). In addition, the idealised LES, though not including these phenomena, predict reasonable z_i compared to the RO. Thus, conclusions for θ can be applied to z_i to first order, consisting more of a plausible scenario than a systematic predictive method for z_i.

5. Similarity theory

Previous sections showed that the LMD Martian Mesoscale/Microscale model is able to reproduce the regional contrasts of BL depth identified in the data. Given this 'validation' and the large range of modelled depths, the LES can be used to derive similarity relationships so as to describe the general structure of the Martian BL.

5.1. *A generalised definition*

It is common in the terrestrial BL literature to analyse the convective BL properties through dimensionless quantities. Adopting the same approach on Mars would obviously help to compare both environments, as first acknowledged by Sorbjan (2007) who noticed the lack of dimensionless analysis in the existing Martian LES literature. Diagnostics in Sorbjan (2007) are based on late-morning LES experiments with idealised radiative heating rates and the Boussinesq approximation. We propose here to refine this preliminary dimensionless study by an analysis of the entire daytime growth of the Martian convective BL, based on LES results with comprehensive radiative transfer and compressible dynamics proved to be in fair agreement with recent RO measurements by H08.

An important prerequisite is to know whether or not formulae developed for the terrestrial convective BL are still applicable to Mars. The answer is clearly no–but the definitions need to be generalised to match the distinct physics of both planets. Knowledge of the Martian BL further illustrates the definition given by Stull (1988): the BL is the part of the atmosphere influenced by the *presence* of the surface, and not only by the surface itself.

On Earth the daytime BL warms 'from below' by the sensible heat flux incoming from the heated surface (Eq. (4)). Thus $\langle w'\theta'\rangle_{\max} = \langle w'\theta'\rangle_0$, where $\langle w'\theta'\rangle_0$ is the near-surface turbulent heat flux. On Mars the daytime BL warms 'from inside and from below' respectively by the infrared radiative heating (plus the visible absorption by the dust) and the sensible heat flux (Eq. (8)). Thus $\langle w'\theta'\rangle_{\max} \neq \langle w'\theta'\rangle_0$. In the Martian environment, the energy that fuels the thermals does not originate only from the atmospheric levels immediately close to the surface. Use of the near-surface heat flux $\langle w'\theta'\rangle_0$ in the convective velocity scale w_*:

$$w_* = \left[g\, z_\mathrm{i}\, \frac{\langle w'\theta'\rangle_0}{\langle\theta\rangle} \right]^{1/3} \tag{11}$$

appears less relevant in the case of Mars.

Physically, the vertical wind scale w_* represents the typical mean value for the BL convective motions. Compared to the resolved Martian thermals in the LES (Figure 5 shows maximum values of vertical winds), such value is underestimated when Eq. (11) is used to compute w_*. More consistent results are obtained if the following general formula (valid both on Earth and Mars) is used:

$$W_* = \left[g\, z_\mathrm{i}\, \frac{\langle w'\theta'\rangle_{\max}}{\langle\theta\rangle} \right]^{1/3}. \tag{12}$$

Similarly, $\langle w'\theta'\rangle_{\max}$ should be substituted for $\langle w'\theta'\rangle_0$ in all dimensionless formulae for the daytime BL.

Convective velocity scales obtained in the five LES cases studied in this paper are shown in Figure 9. Owing to the definition of W_*, conclusions are similar to those in the heat flux analysis in section 3. However, the quantity W_* provides a more direct and intuitive insight into the BL convective motions. While typical values on Earth hardly reach $W_* \sim w_* = 2\,\mathrm{m\,s^{-1}}$ (Stull, 1988), the Martian case exhibits far more vigorous convection with $W_* = 4$ to $6.5\,\mathrm{m\,s^{-1}}$. This is in agreement with the Viking estimates by Sutton *et al.* (1978) and Martínez *et al.* (2009).

5.2. *Mixed-layer relationships for Mars (and comparison with the Earth)*

Similarity laws can be derived by taking advantage of both the temporal evolution of the BL convection and its regional variations (Figure 2). Figure 10 shows the vertical variations of vertical eddy heat flux and vertical velocity variance in the BL in dimensionless form:

$$\frac{\langle w'\theta'\rangle}{\langle w'\theta'\rangle_{\max}} = \mathcal{F}\Big(\frac{z}{z_\mathrm{i}}\Big) \qquad \text{and} \qquad \frac{\langle w'^2\rangle}{{W_*}^2} = \mathcal{V}\Big(\frac{z}{z_\mathrm{i}}\Big).$$

The profiles every 100 s between 1100 and 1600 LT for cases *a*, *b*, *c*, *i* and *z* are superimposed.

Existence of a generic 'mean' profile for the Martian BL convection statistics in quasi-steady midday conditions is shown by Figure 10. Dimensionless vertical structures for potential temperature flux and vertical velocity variance are qualitatively close to LES results by Sorbjan (2007) with idealised radiative forcing (his Figures 3 and 10). Similar figures (not shown) are obtained for each of the five cases *a*, *b*, *c*, *i* and *z* displayed separately. Figure 10 is novel in Martian studies because it combines LES results validated against BL depth measurements in five different regions.

Similarity relationships identified in Figure 10 can be described through the empirical functions

$$\mathcal{F}_\mathrm{M}(x) = \begin{cases} \left(-\frac{3.85}{\ln x} + 0.07 \ln x\right) \mathrm{e}^{-4.61x}, & 0 < x \leq 0.3 \\ -1.52x + 1.24\,, & 0.3 \leq x \leq 1 \end{cases}$$

$$\mathcal{V}_\mathrm{M}(x) = 2.05\, x^{2/3} (1 - 0.64\, x)^2, \qquad 0 < x \leq 1.$$

Martian functions $\mathcal{F}_\mathrm{M}$ and $\mathcal{V}_\mathrm{M}$ are reproduced in Figure 11. Typical empirical equivalents for the Earth,

$$\mathcal{F}_\mathrm{E}(x) = -\,1.2\, x + 1\,, \qquad 0 < x \leq 1$$

$$\mathcal{V}_\mathrm{E}(x) = 1.8\, x^{2/3}\, (1 - 0.8\, x)^2, \qquad 0 < x \leq 1$$

are superimposed (Stull, 1988).

While the terrestrial heat flux is a maximum near the surface, the Martian heat flux is a maximum around $0.1\, z_\mathrm{i} - 0.15\, z_\mathrm{i}$ (i.e. few hundreds of metres above the surface). This is due to the prominent radiative contribution in the BL energy budget, as discussed in section 4. Convective processes act to cool the atmosphere rather than warm it as it is the case on Earth, hence the increase of turbulent heat flux $\langle w'\theta'\rangle$ between the surface and $z \sim 0.1\, z_\mathrm{i} - 0.15\, z_\mathrm{i}$. The heat flux at the Martian surface is only $\langle w'\theta'\rangle_0 \sim 0.15\, \langle w'\theta'\rangle_{\max}$. Thus the need to use the generalised Eq. (12) instead of the Eq. (11) is further confirmed. Above $0.3\, z_\mathrm{i}$, the vertical eddy heat flux decreases linearly with height and becomes negative around $0.8\, z_\mathrm{i}$ both on the Earth and on Mars.

In the vertical variance plot (Figure 11(b)), we find that not only W_*, as shown in Figure 9, but also the ratio $\langle w'^2\rangle / {W_*}^2$ is larger on Mars. Thus the Martian BL is both more buoyant (enhanced W_*) and more responsive to the buoyancy flux (enhanced $\langle w'^2\rangle / {W_*}^2$) than the terrestrial BL. The peak in vertical velocity variance occurs higher in the BL on Mars ($0.4\, z_\mathrm{i}$) than on Earth ($0.3\, z_\mathrm{i}$).

Martian empirical similarity relationships provide a rigorous dimensionless framework for comparisons with the terrestrial convective BL. Other potential applications are numerous (e.g. new BL parametrisations). Only a little information is necessary to compute the convective BL structure at a particular place. Two caveats must be eventually mentioned. Firstly, the generic mean profile remains an empirical approximation only valid in quasi-steady midday conditions. Secondly, an additional parameter is necessary in Martian similarity analysis to acccount for the influence of radiation, a difficulty mentioned in Sorbjan (2007). The scaling proposed in the present paper necessitates the estimation of maximum heat flux $\langle w'\theta'\rangle_{\max}$ which is not given *a priori*.

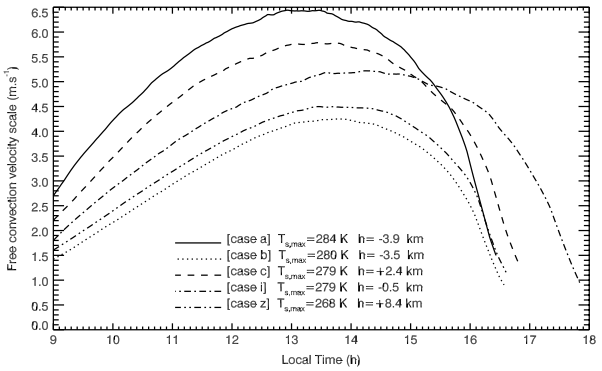

Figure 9. Variations of the convective scaling velocity W_* with time in the five LES case-studies. Values of W_* are computed according to the generalised Eq. (12).

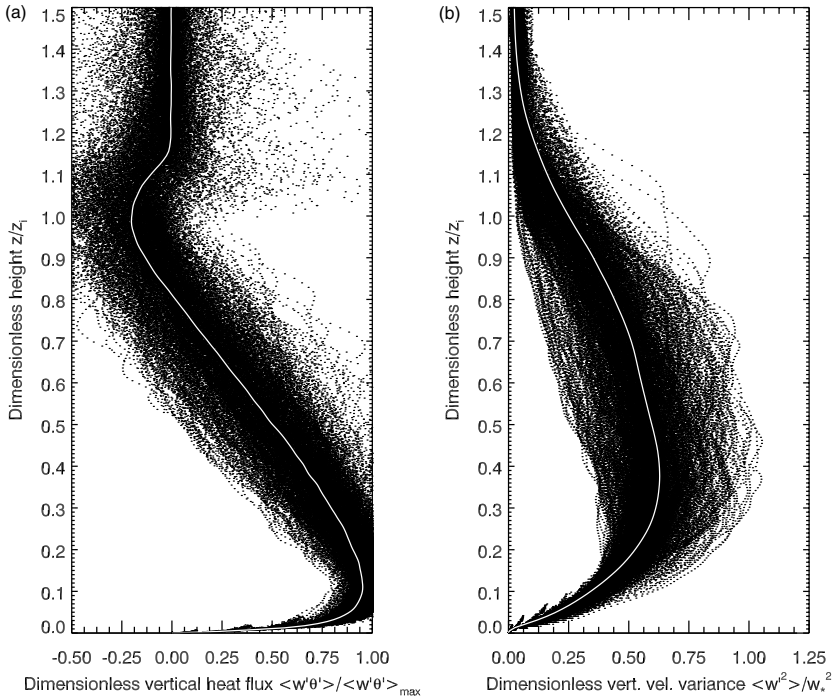

Figure 10. Variations with height of (a) vertical eddy heat flux and (b) vertical velocity variance on Mars. Heat flux, variance and height are normalised respectively by the maximum vertical eddy heat flux, the convective velocity scale W_* (Figure 9) and the boundary layer depth z_i (Figures 2 and 3). The profiles every 100 s between 1100 and 1600 LT for cases *a*, *b*, *c*, *i* and *z* are superimposed, and the average profile is shown as a white line.

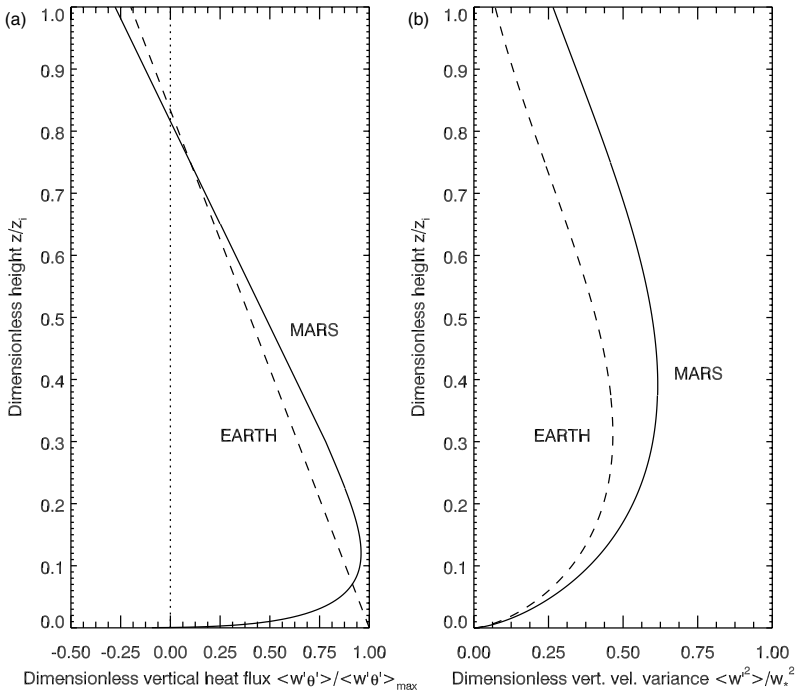

Figure 11. Similarity empirical functions in quasi-steady midday conditions: average variation with dimensionless height of dimensionless (a) vertical eddy heat flux and (b) vertical velocity variance on Mars (solid line) and on the Earth (dashed line).

6. Conclusion

6.1. Summary

The LESs carried out with the LMD mesoscale/micro-scale model quantitatively reproduce the strong regional variations of the afternoon BL depth identified in the RO. The model complements the data by resolving the whole convective BL growth and by giving access to quantities such as vertical velocity, heat flux, and turbulent kinetic energy. Under specific conditions, both the model and the measurements show a positive correlation between surface topography and BL depth.

Our interpretation is that this behaviour is caused by the dominant infrared BL heating rate being fairly independent of elevation (thus near-surface pressure) on Mars. The potential temperature of the mixed layer is then by definition correlated to the inverse pressure ('pressure

effect'). This proposed scenario is supported by the modelled and measured BL potential temperature, though further analysis shows the sensible heat contribution should not be neglected.

The behaviour of the Martian BL, in contrast to the terrestrial one owing to the strong radiative control on Mars, implies a generalised formulation for the BL dimensionless quantities. Taking advantage of this new formulation and the variety of BL depths simulated by the LES, novel empirical similarity relationships for the Martian convective BL are derived. Rigorous comparison between Mars and the Earth and fast computations of the mean Martian BL turbulent statistics are now made possible by such findings.

6.2. *Perspectives*

In spite of their idealised character, the LESs demonstrate good performance in reproducing the measured BL depths. Future work will focus on the effects of variations of dust opacity, background wind, and synoptic/mesoscale vertical motions, so as to yield more realistic LES results. Our paper presents only a sample of the useful diagnostics the LES might provide. For instance, further similarity laws for the Martian convective BL could be derived. Regional variations of convective vortex activity might be investigated and compared to parametrised activity computed from Renno *et al.* (1998) scaling theory. Based on the LES 'reference', an assessment of the performance of the SGS BL parametrisations in GCM and mesoscale models should be of interest too (e.g. Barnes *et al.*, 2008).

Additional conclusions might be also obtained from further exploration of the RO dataset, for instance, our considerations on the 'pressure effect' stand in theory for any spatial/temporal variations of near-surface pressure, not only those induced by the topography. Thus it would be worth investigating if the RO show a seasonal cycle of BL depth at a given location caused by the large variations of pressure induced by CO_2 condensation.

Studying the Martian BL dynamics is crucial to evaluate the possible atmospheric hazards occurring in the (robotic or human) exploration of the Red Planet. Of equal importance is the original point of view that Martian BL studies could bring to BL meteorology in general. To fulfil these purposes, interactions between mesoscale/microscale models and extended observational datasets are required. Thus the inclusion of atmospheric instruments (meteorological towers, *in situ* sensors, orbital sounders) on board the upcoming missions to Mars is critical.

Acknowledgements

We would like to express our gratitude to two anonymous reviewers for rigorous reviews and insightful comments which improved the paper. The project benefited from discussions with colleagues of the 'EuroMars' consortium, the LMD/LATMOS 'Planetary Atmospheres' team and the ISSI 'Mars Boundary Layer' working group. LES runs were carried out on the CICLAD cluster at Institut Pierre-Simon Laplace; we are grateful to F. Bongat and P. Weill for help with computer resources. AS, FF and SRL acknowledge support from European Space Agency (ESTEC TRP contract 11369) and Centre National d'Études Spatiales. AS thanks École Polytechnique for support through a postdoctoral fellowship at an early stage of this project.

References

Barnes JR, Tyler D, Hinson DP. 2008. 'The depth of the daytime convective boundary layer on Mars: A case of extremes'. *LPI Contrib.* **1447**: http://www.lpi.usra.edu/meetings/modeling2008/pdf/9076.pdf.

Blumsack SL, Gierasch PJ, Wessel WR. 1973. An analytical and numerical study of the Martian planetary boundary layer over slopes. *J. Atmos. Sci.* **30**: 66–82.

Briggs G, Klaasen K, Thorpe T, Wellman J. 1977. Martian dynamical phenomenon during June–November 1976: Viking orbiter imaging results. *J. Geophys. Res.* **82**: 4121–4149.

Deardorff JW. 1980. Stratocumulus-capped mixed layers derived from a three-dimensional model. *Boundary-Layer Meteorol.* **18**: 495–527, DOI: 10.1007/BF00119502.

Forget F, Hourdin F, Fournier R, Hourdin C, Talagrand O, Collins M, Lewis SR, Read PL, Huot JP. 1999. Improved general circulation models of the Martian atmosphere from the surface to above 80 km. *J. Geophys. Res.* **104**: 24155–24176.

Forget F, Spiga A, Dolla B, Vinatier S, Melchiorri R, Drossart P, Gendrin A, Bibring JP, Langevin Y, Gondet B. 2007. Remote sensing of surface pressure on Mars with the Mars Express/OMEGA spectrometer: 1. Retrieval method. *J. Geophys. Res. (Planets)* **112**(E11): DOI: 10.1029/2006JE002871.

Gierasch PJ, Goody RM. 1968. A study of the thermal and dynamical structure of the Martian lower atmosphere. *Planet. Space Sci.* **16**: 615–646.

Goody R, Belton MJS. 1967. Radiative relaxation times for Mars. A discussion of Martian atmospheric dynamics. *Planet. Space Sci.* **15**: 247–256.

Haberle RM, Pollack JB, Barnes JR, Zurek RW, Leovy CB, Murphy JR, Lee H, Schaeffer J. 1993. Mars atmospheric dynamics as simulated by the NASA/Ames general circulation model. 1: The zonal-mean circulation. *J. Geophys. Res.* **98**(E2): 3093–3124.

Hess SL, Henry RM, Leovy CB, Ryan JA, Tillman JE. 1977. Meteorological results from the surface of Mars: Viking 1 and 2. *J. Geophys. Res.* **82**: 4559–4574.

Hinson DP, Flasar M, Simpson RA, Twicken JD, Tyler GL. 1999. Initial results from radio occultation measurements with Mars global surveyor. *J. Geophys. Res.* **104**: 26997–27012.

Hinson DP, Pätzold M, Tellmann S, Häusler B, Tyler GL. 2008. The depth of the convective boundary layer on Mars. *Icarus* **198**: 57–66, DOI: 10.1016/j.icarus.2008.07.003.

Lewis SR, Read PL. 2003. Equatorial jets in the dusty Martian atmosphere. *J. Geophys. Res. (Planets)* **108**: 5034, DOI: 10.1029/2002JE001933.

Lilly DK. 1962. On the numerical simulation of buoyant convection. *Tellus* **14**(2): 148–172.

Malin MC, Edgett KS. 2001. Mars Global Surveyor Mars Orbiter Camera: Interplanetary cruise through primary mission. *J. Geophys. Res.* **106**: 23429–23570, DOI: 10.1029/2000JE001455.

Martínez G, Valero F, Vázquez L. 2009. Characterization of the Martian convective boundary layer. *J. Atmos. Sci.* **66**: 2044–2058.

Michaels TI, Rafkin SCR. 2004. Large-eddy simulation of atmospheric convection on Mars. *Q. J. R. Meteorol. Soc.* **130**: 1251–1274.

Michaels TI, Rafkin SCR. 2008. Meteorological predictions for candidate 2007 Phoenix Mars Lander sites using the Mars Regional Atmospheric Modeling System (MRAMS). *J. Geophys. Res. (Planets)* **113**(E12): DOI: 10.1029/2007JE003013.

Millour E, Forget F, Lewis SR. 2008. 'Mars Climate Database v4.3 Detailed Design Document'. Available on http://web.lmd.jussieu.fr/forget/dvd/docs.

Moeng C, Dudhia J, Klemp J, Sullivan P. 2007. Examining two-way grid nesting for large-eddy simulation of the PBL using the WRF model. *Mon. Weather Rev.* **135**(6): 2295–2311.

Montmessin F, Forget F, Rannou P, Cabane M, Haberle RM. 2004. Origin and role of water ice clouds in the Martian water cycle as inferred from a general circulation model. *J. Geophys. Res. (Planets)* **109**: E10004, DOI: 10.1029/2004JE002284.

Pollack JB, Leovy CB, Mintz YH, van Camp W. 1976. Winds on Mars during the Viking season – Predictions based on a general circulation model with topography. *Geophys. Res. Lett.* **3**: 479–482.

Rafkin SCR, Haberle RM, Michaels TI. 2001. The Mars Regional Atmospheric Modeling System: Model description and selected simulations. *Icarus* **151**: 228–256.

Rafkin SCR, Michaels TI. 2003. Meteorological predictions for 2003 Mars Exploration Rover high-priority landing sites. *J. Geophys. Res.* **108**(E12): DOI: 10.1029/2002JE002027.

Renno NO, Burkett ML, Larkin MP. 1998. A simple thermodynamical theory for dust devils. *J. Atmos. Sci.* **55**: 3244–3252.

Richardson MI, Toigo AD, Newman CE. 2007. PlanetWRF: A general purpose, local to global numerical model for planetary

atmospheric and climate dynamics. *J. Geophys. Res.* **112**(E09001): DOI: 10.1029/2005JE002636.
Savijärvi H. 1999. A model study of the atmospheric boundary layer in the Mars Pathfinder lander conditions. *Q. J. R. Meteorol. Soc.* **125**: 483–493.
Savijärvi H, Mä ättänen A, Kauhanen J, Harri A-M. 2004. Mars Pathfinder: New data and new model simulations. *Q. J. R. Meteorol. Soc.* **130**: 669–683.
Schofield JT, Crisp D, Barnes JR, Haberle RM, Magalhães JA, Murphy JR, Seiff A, Larsen S, Wilson G. 1997. The Mars Pathfinder Atmospheric Structure Investigation/Meteorology (ASI/MET) experiment. *Science* **278**: 1752–1757.
Skamarock WC, Klemp JB. 2008. A time-split non-hydrostatic atmospheric model for weather research and forecasting applications. *J. Comput. Phys.* **227**: 3465–3485, DOI: 10.1016/j.jcp.2007.01.037.
Smith EA, Shi L. 1992. Surface forcing of the infrared cooling profile over the Tibetan Plateau. Part I: Influence of relative longwave radiative heating at high altitude. *J. Atmos. Sci.* **49**: 805–822.
Smith MD, Pearl JC, Conrath BJ, Christensen PR. 2001. Thermal Emission Spectrometer results: Mars atmospheric thermal structure and aerosol distribution. *J. Geophys. Res.* **106**(E4): 23929–23945. DOI: 10.1029/2000JE001321.
Smith MD, Wolff MJ, Spanovich N, Ghosh A, Banfield D, Christensen PR, Landis GA, Squyres SW. 2006. One Martian year of atmospheric observations using MER Mini-TES. *J. Geophys. Res. (Planets)* **111**(E10): DOI: 10.1029/2006JE002770.
Sorbjan Z. 2007. Statistics of shallow convection on Mars based on large-eddy simulations. Part 1: Shearless conditions. *Boundary-Layer Meteorol.* **123**: 121–142. DOI: 10.1007/s10546-006-9128-7.
Spiga A, Forget F. 2009. A new model to simulate the Martian mesoscale and microscale atmospheric circulation: Validation and first results. *J. Geophys. Res. (Planets)* **114**(E13): DOI: 10.1029/2008JE003242.
Stull RB. 1988. *An introduction to boundary-layer meteorology*. Kluwer Academic: Dordrecht, the Netherlands.
Sutton JL, Leovy CB, Tillman JE. 1978. Diurnal variations of the Martian surface layer meteorological parameters during the first 45 sols at two Viking lander sites. *J. Atmos. Sci.* **35**: 2346–2355.
Thomas P, Gierasch PJ. 1985. Dust devils on Mars. *Science* **230**: 175–177.
Toigo AD, Richardson MI. 2003. Meteorology of proposed Mars Exploration Rover landing sites. *J. Geophys. Res.* **108**(E12): DOI: 10.1029/2003JE002064.
Toigo AD, Richardson MI, Ewald SP, Gierasch PJ. 2003. Numerical simulation of Martian dust devils. *J. Geophys. Res. (Planets)* **108**: 5047, DOI: 10.1029/2002JE002002.
Tyler D, Barnes JR, Skyllingstad ED. 2008. Mesoscale and large-eddy simulation model studies of the Martian atmosphere in support of Phoenix. *J. Geophys. Res. (Planets)* **113**(E12): DOI: 10.1029/2007JE003012.
Wilde NP, Stull RB, Eloranta EW. 1985. The LCL zone and cumulus onset. *J. Appl. Meteorol.* **24**: 640–657.
Ye ZJ, Segal M, Pielke RA. 1990. A comparative study of daytime thermally induced upslope flow on Mars and Earth. *J. Atmos. Sci.* **47**: 612–628.

